Astron. Astrophys. 336, 329–338 (1998)

ASTRONOMY AND ASTROPHYSICS

The Cometary Globules CG 30/31/38 in the Gum nebula

A radio line spectroscopic investigation⋆

A.S. Nielsen[1], **M. Olberg**[2], **J. Knude**[1], **and R.S. Booth**[2]

[1] Niels Bohr Institute for Astronomy, Physics and Geophysics, Astronomical Observatory, DK-2100 Copenhagen, Denmark
[2] Onsala Space Observatory, S-439 00 Onsala, Sweden

Received 17 July 1996 / Accepted 24 April 1998

Abstract. We present radio line observations from the SEST. On the basis of ^{13}CO (J=1–0) measurements we estimate the H_2 mass associated with the globules CG 30/31A-C/38 to be $\sim$43 $M_\odot$. The gas kinetic temperature of the globules is in the range 5 to 14 K. Line wings seen in the ^{12}CO spectra as well as higher dipole moment molecules towards CG 30, indicate that a dense molecular outflow is present. Especially the red wing reveals itself very clearly and is collimated, whereas the blue wing is weak and the emission is smeared out. The mass of the outflow is $\sim$0.3 $M_\odot$ and the dynamical time scale is 1.7×10^4 years. The mechanical luminosity is 0.11 $L_\odot$ for an assumed inclination of 90°. The ^{13}CO (J=1–0) data have revealed that CG 30 is a possible double globule, the small companion (here named CG 30B) having a mass of $\sim$25% of the larger globule, corresponding to $\sim$2 $M_\odot$.

Key words: stars: low-mass, brown dwarfs – stars: formation – ISM: individual objects: CG30 – ISM: individual objects: CG31 – ISM individual objects: CG38 – ISM: kinematics and dynamics

1. Introduction

Bok globules are among the smallest entities that are known to form individual and/or binary low mass stars. The typical size of the globules is in the range 0.1–0.8 pc and their mean densities are high, 10^4–10^5 cm^{-3}. The temperature in the cores is around 10 K, and the mass contained in the globules is less than 100 $M_\odot$. A fraction of these globules, first described and defined as a group by Hawarden & Brand (1976) based on Schmidt plates of the Gum nebula and NGC 5367, is known as cometary globules (CG's) due to their striking resemblance to solar system comets. The head of a CG is a dense dark cloud consisting of gas and dust of opacity class A, defined as clouds through which no background stars are visible (Hartley et al. 1986). Class A is equivalent to the opacity class 6 defined by Lynds (1962). On the side opposite to the ionising sources, a long faintly luminous tail prolong the globule. The head is often associated with a bright rim of photo-evaporated material (Pottasch 1956) due to the incident radiation from nearby early type stars, which always are found to be associated with cometary globules.

Reipurth (1983) proposed a possible scenario for the formation of the cometary globules, according to which cometary globules originate as cloud cores in larger molecular clouds, of which the more tenuous parts are destroyed by strong UV radiation from OB stars. If the globules do not fully evaporate in the lifetime ($\sim10^6$ yr) of the UV source(s), they will eventually relax and diffuse into the general interstellar medium.

The formation and evolution of cometary globules due to radiation driven implosions (RDI) was treated analytically by Bertoldi (1989) and Bertoldi & McKee (1990). The RDI model is based on the 'rocket effect' introduced by Oort & Spitzer (1955), whereby the ionised gas expands into the interstellar medium and an ionisation front preceded by a shock in the neutral gas propagates into the cloud. This shock may well trigger the formation of a star in the head of the cometary globule. This scenario has recently been supported by Lefloch & Lazareff (1994, 1995) discussing the RDI model in much more detail than previously, using both numerical hydrodynamics and simple analytical modelling.

1.1. CG's in the Gum nebula

It is well established, that the Gum nebula contains at least 32 cometary globules (Reipurth 1983; Zealey et al. 1983). The Gum nebula itself is a large shell structure having a radius of 18° seen in deep Hα and [NII] emission, first recognised as an entity by Gum (1952). There have been several different suggestions for the origin of the Gum nebula: Gum (1952) proposed it to be an extended H II region; Brandt et al. (1971) argued that it was initially heated by a supernova outburst. Recently, Sahu (1992) has concluded that the nebula is a shell structure formed by the interaction of the stars in the Vela R2 association with the surrounding ISM through ionising radiation, stellar winds and supernova explosions. Whether the nebula is expanding has also been a subject of controversy, but recent work, Sridharan (1992), on the kinematics of the CG's in the Gum nebula, favours expansion of the nebula with an inferred velocity of 12

Send offprint requests to: A.S. Nielsen, (alan@astro.ku.dk)

⋆ Based on observations collected at the European Southern Observatory, La Silla, Chile.

km s^{-1}. In the IRAS maps Sahu (1992) found an extended shell around the Vela OB2 association coincident with the ring of the cometary globules. The expansion of the ionised gas in the IRAS Vela shell, probably caused by stellar winds and supernova explosions in Vela OB2, is 10 ± 2 km s^{-1}, comparable to the expansion velocity of the Gum nebula.

The distances to the CG's, essential for the computed physical parameters are uncertain since only indirect estimates exists. An assumed value of 450 pc is normally used and has also been used in this work. Besides the cometary globules, the nebula contains numerous dark clouds. However, while some of the dark clouds in this area could be outside the Gum nebula the orientation of the cometary tails of the CG's suggests that all the CG's are influenced by the Gum nebula (Bhatt 1993). The tails of the CG's point toward the centre of the Gum nebula situated in the middle of a triangle outlined by the three powerful sources: ζ-Puppis (O4f), γ^2-Velorum (WC8+O9I) and the Vela Pulsar, suggesting a common origin of the cometary shape (Zealey et al. 1983). The three sources are sufficient to maintain the ionisation of the Gum nebula. The angular separation of the globules from the central region, varies between 6.5° and 11.6°, which at 450 pc indicates projected distances between 50 pc and 90 pc. Most of the globules have a projected distance of $\approx$70 pc.

The globules are found at almost all position angles, often in groups, but with a preference for the western part of the Gum nebula. The cometary globules have been extensively observed at optical and near infrared wavelengths (Sandquist 1976; Reipurth 1983; Brand et al. 1983; Pettersson 1984; Graham 1986). These studies show evidence of low mass star formation in the heads of these globules. IRAS has revealed an enhanced star formation rate in the CG's compared to other isolated clouds in the galaxy. Bhatt (1993) concluded that about 50% of the CG's heads are found to have IRAS sources with flux densities increasing with wavelength, characteristic of young stellar objects (YSO's) embedded in dense dust clouds. Furthermore, the luminosities associated with the YSO's are in the range from $\sim$0.5 L$_\odot$ to 20 L$_\odot$, characteristic of low mass YSO's or protostellar objects.

The best known example of a globule with ongoing star formation is the case of the dark cloud ESO 210–6A with its highly collimated string of Herbig-Haro objects, HH 46 and HH 47 (Reipurth & Cernicharo 1995). But there are numerous other examples. Bernes 135 a variable emission line (Hα emission) Herbig Ae/Be star that has been shown to be a pre-main-sequence star formed in CG 1 (Reipurth 1983). CG 30 contains the Herbig-Haro object HH 120 and the IR source CG 30-IRS 4 (Pettersson 1984).

Star formation in the Gum nebula could have been triggered by the event that created the nebula itself. However, it is a complicated task to understand the nature of this event and choose between the models proposed for the Gum nebula (Sahu 1992).

Because of their simple nature and morphology, compared to the much more complicated GMC's, globules are ideal laboratories for studying the conditions leading to the formation of single or binary low mass stars.

2. The data

The observations were made with the Swedish ESO 15 metre sub-millimetre telescope (SEST) on La Silla, Chile in 1988/89, and a new study of the globules was carried out in September 1995. At the time of the observations, the telescope was equipped with a cooled dual channel Schottky mixer receiver for the 80–115 GHz frequency range, with a single side band (SSB) noise temperature of about 300 K giving a resulting system temperature between 400 and 700 K.

The primary purpose in 1988/89 was to look for a molecular outflow around the Herbig-Haro object HH 120 in CG 30, which is known to be associated with star formation. CG 31ABC and CG 38 was fully mapped in the ^{13}CO (J=1–0) line with a 40″ grid spacing. CG 31A has been mapped in ^{12}CO (J=1–0) at 90 positions around the centre position, using a spacing of 40″, whereas CG 31B and CG 31C were both mapped at 9 positions around the centre with a spacing of 20″. Furthermore, the globules have been observed in the CS (J=2–1) and C^{18}O (J=1–0) lines towards the centre position. The integration time was 120 sec, except at the centre position where is was 300 sec. The CS (J=2–1) and C^{18}O (J=1–0) spectra were integrated in 600 sec due to the weak signal in the globules.

Although the ^{12}CO (J=1–0) molecular line profiles in CG 30 showed wing emission, their interpretation was a little uncertain due to the low spatial resolution and partly poor quality of the spectra taken in 1989.

In September 1995, we observed the globules, using the 2 mm and 3 mm Schottky receivers in parallel. With the 2 mm receiver, we obtained spectra of higher dipole moment molecules (CS (J=3–2), H_2CO and C_3H_2) allowing us to investigate the outflow in more detail.

All spectra were obtained using a high resolution acousto optical spectrometer (AOS) with 2000 channels, spaced by 44 kHz ($\sim$0.1 km s^{-1} at the CO (J=1–0) frequency). The HPBW of the SEST at 115 GHz is 43″ and 33″ at 150 GHz (2 mm). The telescope and its associated equipment, have been described by Booth et al. (1989).

The calibration was done with an online temperature controlled chopper wheel. The chopper calibrated spectra obtained with the telescope are in the $T_{\rm A}^*$ temperature scale as defined by Kutner & Ulich (1981), and are corrected for atmospheric attenuation and antenna losses. The antenna temperatures were corrected for forward scattering and spillover by applying $\eta_{\rm fss}$, taken to be 0.92 at all observed frequencies. The corresponding main beam efficiencies are 0.70 and 0.67 at 115 and 150 GHz, respectively. During the observations we checked the telescope pointing by observing a SiO (v=1, J=2–1) maser source. The root-mean-square pointing offset relative to the telescope pointing model was a few arc seconds, and no systematic pointing offsets were noted during the observing runs. We have employed frequency switching of typically 15 or 20 MHz, introducing baseline curvatures, which were corrected for by fitting and subtracting polynomials up to third order, using DRP (Data Reduction Package) developed for the SEST telescope by M. Olberg.

3. Physical parameters

Before proceeding to a discussion of the individual globules and the molecular outflow in CG 30, we briefly discuss the assumptions leading to the physical parameters. They depend on the excitation temperature, the optical depth and the filling factor of the gas. With these parameters, an estimate of the column density as a function of velocity is possible. An expression for the total column density of a linear, rigid rotor molecule under conditions of local thermodynamical equilibrium (LTE), and the assumption that all levels are characterised by a single excitation temperature, $T_{\rm ex}$, is given by (Garden et al. 1991):

$$N_{\rm tot} = \frac{3k}{8\pi^3 B\mu^2}\frac{\exp[hBJ(J+1)/kT_{\rm ex}]}{(J+1)} \times \frac{(T_{\rm ex}+hB/3k)}{[1-\exp(-h\nu/kT_{\rm ex})]}\int \tau_v dv \quad (1)$$

where μ is the permanent dipole moment, and B is the rotational constant of the molecule. In the optically thin case the integrated optical depth is proportional to the integrated antenna temperature

$$\int \tau dv = \frac{1}{\eta_{\rm fss} f(\mathcal{F}(T_{\rm ex})-\mathcal{F}(T_{\rm bg}))}\int T_{\rm A}^* dv \quad (2)$$

$T_{\rm bg}$ is the temperature of the cosmic background radiation which is close to 2.7 K, f is the filling factor where we have used the standard value of 1. $\mathcal{F}_\nu(T) = (h\nu/k)/(\exp(h\nu/kT)-1)$.

In the case that the filling factor f is independent of velocity and is less than 1, e.g 0.5, the derived column densities and masses will be twice as large.

For ^{13}CO the conversion of the measured line intensity into column density becomes

$$N(^{13}{\rm CO}) = 2.41\times10^{14}\frac{(T_{\rm ex}+0.88)}{1-\exp(-5.53/T_{\rm ex})} \times \frac{1}{\eta_{\rm fss} f(\mathcal{F}(T_{\rm ex})-\mathcal{F}(T_{\rm bg}))}\int T_{\rm A}^* dv \quad (3)$$

Unfortunately, it is very difficult (if not impossible) to determine the excitation temperature of ^{13}CO directly. However, earlier observations of NH_3 and CS (Martin & Barrett 1978) have shown that the density in the centre of globules is quite high (10^4–10^5 cm^{-3}), sufficient to imply that ^{12}CO and ^{13}CO are both thermalised. Since the ^{12}CO emission is normally optically thick, it is possible to calculate the excitation temperature (and kinetic temperature) from

$$T_{\rm ex} = T_{\rm kin} = T_0\left[\ln\left(T_0/\left[\frac{T_{\rm A}^*}{\eta_{\rm fss}}+\mathcal{F}(T_{\rm bg})\right]+1\right)\right]^{-1} \quad (4)$$

where $T_0 = h\nu/k$.

Under the assumption that $T_{\rm ex}(^{13}{\rm CO})$=$T_{\rm ex}(^{12}{\rm CO})$= $T_{\rm kin}$ (LTE condition), the opacity in ^{13}CO can be deduced from a comparison with the antenna temperature, $T_{\rm A}^*$

$$\tau(^{13}{\rm CO}) = -\ln\left[1-\frac{T_{\rm A}^*(^{13}{\rm CO})}{T_{\rm A}^*(^{12}{\rm CO})}\right] \quad (5)$$

In the case that ^{12}CO is optically thick and ^{13}CO is optically thin, the two isotopes trace different parts of the cloud, implying that the species need not have the same temperature. If $T_{\rm ex}$(CO)> $T_{\rm ex}(^{13}{\rm CO})$, which could well be the case, especially if we take radiative trapping under consideration, we will underestimate the true value of $\tau(^{13}{\rm CO})$.

We assume that the relative abundance between ^{12}C and ^{13}C is similar to the solar system value of 89 (Kutner 1984), implying that $\tau(^{12}{\rm CO}) = 89\tau(^{13}{\rm CO})$. By assuming that the ratio between ^{13}CO and H_2 is 2.5×10^{-6} (Lada 1985), we can calculate the mass of the globules

$$M = \mu m({\rm H_2})\int_{\mathcal{A}} N({\rm H_2}) d\mathcal{A} \quad (6)$$

where $\mathcal{A}$ is the projected area in cm^2, and μ is the mean molecular weight.

It is important to emphasise, that the mass estimate derived from ^{13}CO column density, depends on the validity of the LTE assumption and the assumed abundances of the CO isotopes. Some processes which could lead to deviations from LTE are subthermal excitation due to low densities, photodissociation and chemical fractionation. While the ^{12}CO emission might be thermalised even at low densities, the less abundant isotopes may be characterised by a lower excitation temperature ($T_{\rm kin} > T_{\rm ex}$) because the density is too low to bring the excitation of the molecule into equilibrium with the thermal motions in the gas. Thus, for subthermally excited emission the kinetic temperature may be larger than the excitation temperature, thereby giving rise to an overestimation of the cloud mass determined by Eqs. (3) and (4).

In addition, the Gum nebula is a region of high UV radiation (Reipurth 1983; Sahu 1992; Sridharan 1992). Because CO and H_2 do not have identical shielding, a larger fraction of CO molecules (relative to H_2) will be destroyed. This effect may result in an underestimate of N(H_2) and the masses.

4. Observational results

We now turn to a detailed discussion of the individual cometary globules and their physical parameters.

In Table 1, the (1950) coordinates for each of our sources are listed, corresponding to the position of maximum ^{12}CO emission. Column 4 ($W_{\rm h}$) is the width of the head of the globule, and column 6 ($L_{\rm h+t}$) is the combined length of the head+tail, for the assumed distance of 450 pc.

4.1. ^{12}CO observations

In Table 2, the observational characteristics of the ^{12}CO emission are listed for all the globules. Column 5 (Δv) is the equivalent width of the line defined as the integrated intensity divided by peak temperature.

From this Table it is noticeable that all the globules, but especially CG 31D and CG 31E, are characterised by low temperature and narrow lines. Furthermore, no wing emission is associated with CG 31/38. This is in agreement with Bhatt (1993), who

Table 1. Centre positions of the cometary globules in the CG 30/31/38 complex (taken from Reipurth 1981).

Source	α (h m s)	δ ($^\circ$ $'$ $''$)	W_h ($'$)	W_h (pc)	$L_\mathrm{h+t}$ (pc)
CG 30	8 07 39	-35 56 20	2.3	0.30	1.27
CG 31A	8 07 10	-35 52 24	2.9	0.38	3.04
CG 31B	8 06 55	-35 54 14	1.4	0.18	0.60
CG 31C	8 06 40	-35 50 44	2.9	0.38	2.62
CG 31D	8 06 24	-35 52 58	0.4	0.05	0.18
CG 31E	8 06 21	-35 55 18	0.3	0.04	0.08
CG 38	8 07 47	-36 01 41	0.8	0.10	0.38

Table 2. ^{12}CO characteristics of the cometary globules towards the centre position (see Fig. 4 for a general overview of the globules).

Source	T_A^* (K)	T_ex (K)	$\int T_\mathrm{A}^* dv$ (K km/s)	Δv (km/s)	v_peak (km/s)
CG 30	8.1	12.2	29.9	3.65	6.0
CG 31A	7.6	11.6	11.8	1.56	5.9
CG 31B	5.7	9.5	6.8	1.20	5.7
CG 31C	9.9	14.2	19.3	1.95	6.1
CG 31D	2.6	6.0	3.1	1.19	6.2
CG 31E	1.9	5.1	2.6	1.37	7.4
CG 38	4.3	7.8	4.8	1.21	6.8

concluded that none of the globules, except CG 30 (discussed in Sect. 4.3), host any infrared point sources or star formation processes.

The excitation temperatures listed in Table 2 have to be considered as upper limits since they are calculated from the centre positions of the globules, where T_A^* is largest.

CG 31A is complex because it is double peaked at the centre position (Fig. 1); one line centred at 6 km s^{-1} (the main line), and a weaker line centred at $\sim$10 km s^{-1}. This weak line reaches a maximum at the offset position (80″,-40″) (abbreviated (80,-40) in the following text) with a peak temperature of 5.6 K, and a width of 1.27 km s^{-1}. Although the ^{12}CO emission from these two lines is present in most of the spectra, some variation seems evident: the line centred at the high velocity, reveals itself mostly in the central region and in the region towards south-east, whereas the main line is present all over but is especially strong in the centre region and to the north-west of the globule. This behaviour of the gas may be explained as a disintegration of the globule, maybe as a result of instabilities caused by strong winds and radiation pressure from the massive stars associated with the Gum nebula. Another explanation could be that we simply have a clump of gas moving at a different velocity than the main part of CG 31A (see also discussion of CG 30 below). CG31 B, CG31 C and CG 38 are associated with one spectral line only.

CG 31D and CG 31E, discussed by Reipurth (1983), are the two smallest globules in the complex, only about half the size of CG 38. They have only been observed at the (0,0) position in ^{12}CO (J=1–0), C^{18}O (J=1–0) and CS (J=2–1) due to their small size (see Fig. 4) and insignificant mass compared to the rest

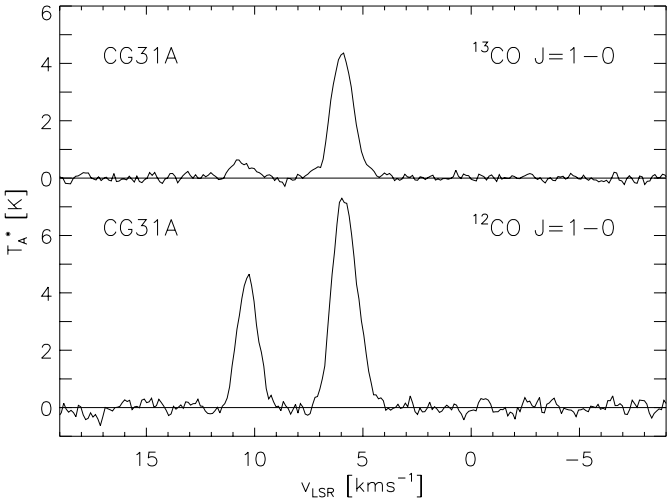

Fig. 1. Spectrum of ^{12}CO and ^{13}CO emission at the centre position of CG 31A. This globule is different from the rest of the globules in the CG 30/31/38 complex, because the emission is double-peaked at the centre position.

Table 3. ^{13}CO line characteristics of the cometary globules towards their centre position.

Source	T_A^* (K)	$\int T_\mathrm{A}^* dv$ (K km/s)	Δv (km/s)	τ	v_peak (km/s)
CG 30	4.0	6.6	1.7	0.7	6.0
CG 31A	4.4	5.8	1.3	0.9	7.0
CG 31B	3.8	2.0	0.5	1.1	6.1
CG 31C	4.7	6.7	1.4	0.6	5.9
CG 38	2.6	2.1	0.8	0.9	6.2

of the globules in the CG 30/31/38 complex. Because of the very sparse observational data we cannot derive the mass of the globules or any other physical parameters.

4.2. ^{13}CO observations

In Table 3 below, we have listed the observed ^{13}CO line characteristics for each of the cometary globules.

4.2.1. CG 38

CG 38 is a small globule in front of the CG 30/31 complex, as seen from the direction of the centre of the Gum nebula (see Fig. 4), and it has a dense head and a bright rim. The globule has been mapped at 5×5 positions with a 40″ spacing. At the assumed distance of 450 pc, it corresponds to 0.35×0.35 pc.

CG 38 is single peaked at the centre position, but in the north-western region, a second line component reveals itself. This line is present in 5 spectra, and in Fig. 2, a spectrum is shown with the maximum emission from this second line, at 10 km s^{-1}. Even though the temperature is only 1.3 K, the line is broader than the main line (at 6 km s^{-1}) with a value of 0.92 km s^{-1}, indicating a more turbulent region compared to the central parts. In Fig. 3, a

Table 4. Physical parameters for the cometary globules in the Gum nebula. S.C is the strong line component at $\sim$6 km s^{-1} and W.C is the weak line component centred at $\sim$10 km s^{-1}. W.C in CG 30 is called CG 30B in Sect. 4.3 and probably represent a new globule, since it is so well defined, which is not the case for the W.C component associated with CG 31A. The sum in column 2 and 3 represents the total observed area.

Source	$\sum\int T_A^* dv$ (K km/s)	$\sum$(N(^{13}CO)) (cm^{-2})	M(H_2) ($M_\odot$)	n(H_2) at (0,0) (cm^{-3})
CG 30 (S.C)	147.37	1.6×10^{17}	7.9	3.6×10^{3}
CG 30 (W.C)	31.15	3.5×10^{16}	1.7	-
CG 30 (Total)	178.52	$\sim2\times10^{17}$	9.6	-
CG 31A (S.C)	277.47	3.0×10^{17}	14.6	2.4×10^{3}
CG 31A (W.C)	35.42	3.9×10^{16}	1.9	-
CG 31A (Total)	312.89	3.4×10^{17}	16.5	-
CG 31B	171.03	1.8×10^{17}	8.7	2.3×10^{3}
CG 31C	131.90	1.6×10^{17}	7.5	3.1×10^{3}
CG 38	11.6	1.2×10^{16}	0.6	2.2×10^{3}

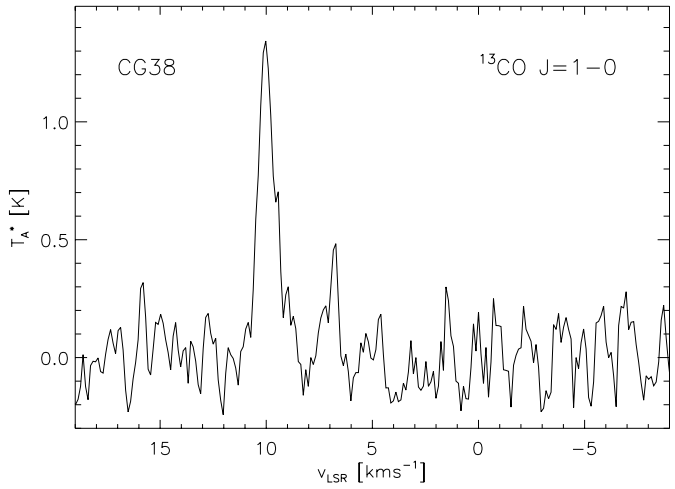

Fig. 2. Spectrum of ^{13}CO emission at the (-40,40) position of CG 38. The second line component at v $\sim$10 km s^{-1} is clearly seen at this position, whereas the main line at 6 km s^{-1} is completely absent.

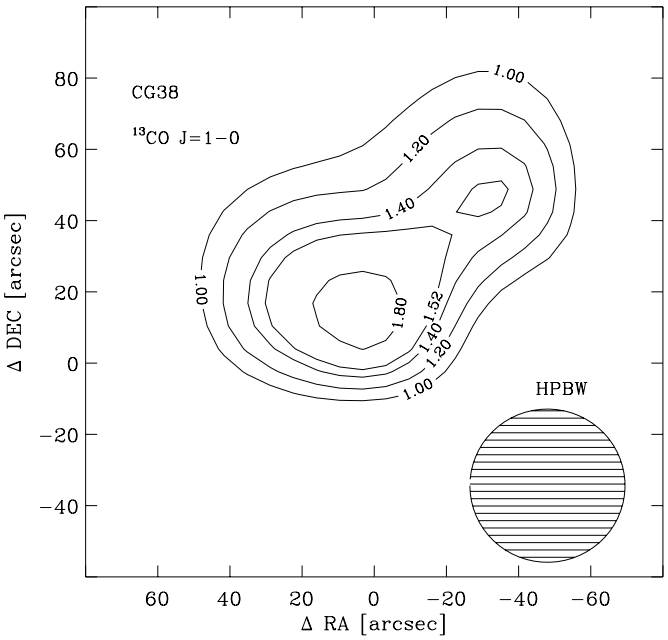

Fig. 3. Smoothed ^{13}CO emission contour plot of CG 38. The line component at 10 km s^{-1} emission peaks at (-40,40).

smoothed contour plot of the ^{13}CO emission clearly shows two distinct velocity components. The globule is seen to be double-peaked. We think that this should be explained by a motion of matter away from the globule; in other words, the globule is disintegrating. In principle the two peaks could be explained by systematic motions such as rotation. However, rotation is not a common phenomenon associated with globules in general (Leung et al. 1982). Following the method described in Sect. 3, we have derived the physical parameters for CG 38, which are listed in Table 4. The density at the central position can be estimated if we assume that the globule is a homogeneous sphere with a diameter of 0.1 pc. As the diameter used is an upper limit, we may consider the density estimate to be a lower limit. The derived density is too low to account for the CS and C^{18}O intensities obtained at the centre position (see below), which could mean that CG 38 is shallower than assumed, but more probably clumpiness accounts for the strength of the higher dipole moment molecule. However, higher resolution observations are needed in order to constrain the physical properties of CG 38.

4.2.2. CG 31A

CG 31A has been observed at 104 different positions in ^{13}CO around the centre position covering the whole globule.

In Fig. 1, a spectrum of the ^{13}CO emission at the centre position is shown, and like the ^{12}CO emission, two lines appear. But the intensity ratio at the centre position, is significantly larger for the ^{13}CO than for the ^{12}CO emission. For the ^{13}CO emission the ratio is 8:1, and for the ^{12}CO emission it is 2:1, indicating a smaller mass associated with the second line component (see Table 4).

The ^{13}CO emission is confined to an area smaller than the ^{12}CO emission, as expected. But we also notice the same kind of velocity structure as for ^{12}CO: when we move from the north-west towards south-east, the main component becomes increasingly stronger. It reaches its maximum at the (120,-40) position,

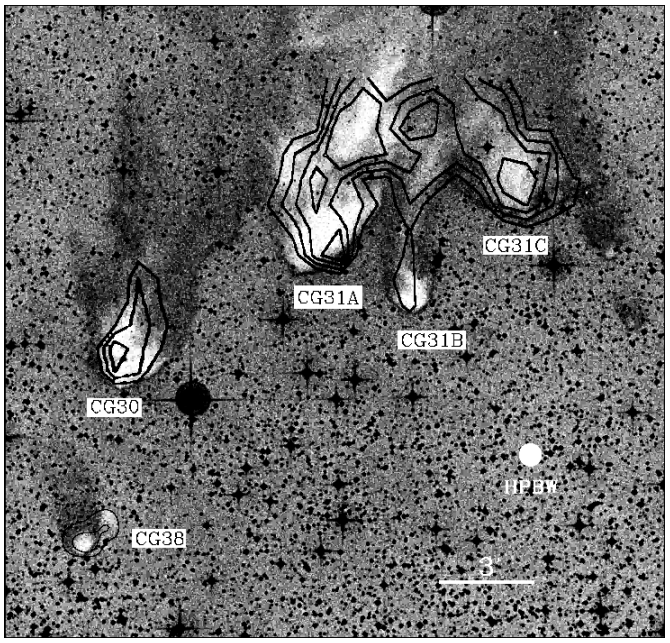

Fig. 4. Contour plot of ^{13}CO emission (line component at $\sim$6 km s^{-1}) associated with CG 30/31ABC/38 in the Gum nebula superposed on an optical picture. Contour levels start at 2.5 K kms^{-1} in steps of 1 K kms^{-1}. CG 38 is indicated by two contours corresponding to 1 K kms^{-1} and 1.5 K kms^{-1}. CG 31D and CG 31E can be seen in the direction south-west of CG 31C. The contours are drawn with IDL and the optical picture is from Digital Sky Survey.

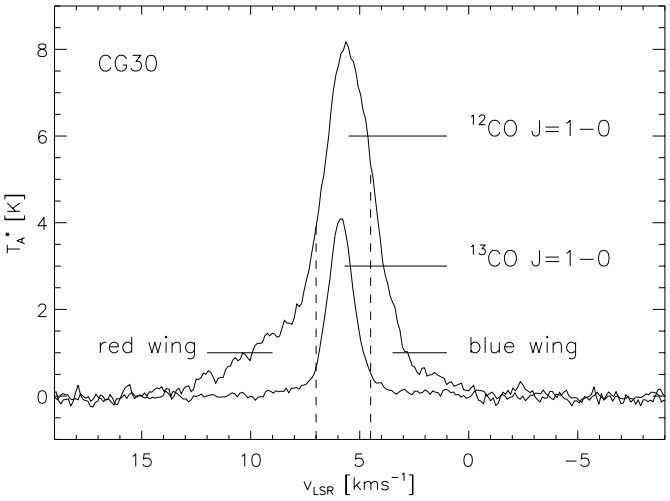

Fig. 5. ^{13}CO superposed on the ^{12}CO spectrum of CG 30 towards the centre position. The two lines (both J=1–0) are scaled to the same temperature range. Between the dashed lines, from 4.5 to 7 km s^{-1} (3σ-level) only core emission is present. A red wing clearly reveals itself in the velocity interval from 7 to 15 km s^{-1}, whereas the blue wing is less prominent from -2 to 4.5 km s^{-1}.

which also seems to be the case for the ^{12}CO emission, with a peak antenna temperature of 0.8 K, and a width of 0.83 km s^{-1}.

The results obtained for the ^{13}CO emission, are presented in Table 4. The *strong component* (S.C) has been integrated over the velocity range from 3 to 8.5 km s^{-1}, and the *weak component* (W.C) from 9 to 13 km s^{-1}.

4.2.3. CG 31B and CG 31C

CG 31B was mapped in ^{13}CO at 5×14 different positions, because of its very elongated structure (Fig. 4). This globule is associated with one line component only. However, due to uncertainties, and the assumption of spherical structure, the similarity of the values of $n(H_2)$ (Table 4) for CG 31A and CG 31B is more a coincidence than a reflection of the real physical conditions. Like CG 31B, CG 31C is characterised by one spectral line only. CG 31C is larger than CG31 B, but according to our mass estimate more mass is contained in CG31 B, indicating that CG 31C is more centrally condensed than CG31 B.

4.3. CG 30

CG 30 is among the largest cometary globules in the complex, with an angular diameter of nearly 2.3′ which at an assumed distance of 450 pc, corresponds to 0.3 pc.

CG 30 hosts an infrared object, IRS 4 and a related Herbig-Haro object, HH 120 (Pettersson, 1984).

4.3.1. ^{13}CO observations

We mapped CG 30 at 82 positions spaced by 40″. At the (-40,0) position the temperature is 4.6 K, even higher than at the centre position (see Table 3). Some of the spectra show two distinct line components, as in CG 31A and CG 38. Again, the second line component is centred at 10 km s^{-1}, and is only visible in the north and north-western parts of the globule. It has a maximum at (0,160) (Fig. 7) where the peak temperature is $T_A^* = 2.0$ K. When moving in the northern direction we do not find any sign of velocity gradients in the main line and we therefore suggest that this second line traces a mass component detached from CG 30, in a similar same way as in the case of CG 31A and CG 38.

None of the ^{13}CO emission profiles seems to be associated with any sign of wing emission at all.

4.3.2. ^{12}CO observations

CG 30 has been mapped at 147 positions with a 20″ grid spacing, covering an area of approximately 0.48×0.61 pc at the assumed distance of 450 pc. Fig. 5 shows a plot of the ^{12}CO and ^{13}CO emission towards the centre of CG 30. A broad red wing is clearly seen in the velocity interval from 7 to 15 km s^{-1}, as well as a less pronounced blue wing in the velocity interval from -2 to 4.5 km s^{-1}. Normally, wing emission is not expected in the ^{13}CO spectra, unless the molecular outflow is extremely powerful. We consequently assume that the ^{13}CO emission originates in the core only. We can then determine the velocity range for the wing emission, assuming that the ^{13}CO and ^{12}CO core emission have the same velocity extent (see Fig. 5).

Table 5. CS (J=2–1) and $C^{18}O$ (J=1–0) observations for the globules and the Gum dark clouds (GDC's) towards the centre position T_p is the peak temperature and v_p is the peak velocity.

	CS			$C^{18}O$		
Source	T_p (K)	v_p (km/s)	Δv (km/s)	T_p (K)	v_p (km/s)	Δv (km/s)
CG 30	2.37	5.66	1.47	0.87	5.38	0.88
CG 31A	1.93	5.53	0.89	1.00	5.38	0.79
CG 31B	1.64	5.41	0.64	0.86	5.28	0.50
CG 31C	1.15	5.83	0.87	0.82	5.68	0.75
CG 38	0.71	6.50	0.61	0.31	6.39	0.31
GDC 1	1.54	4.66	0.92	1.01	4.66	0.68
GDC 2	1.49	5.30	0.84	0.87	5.31	0.69
GDC 3	0.65	5.22	0.57	0.20	5.37	0.40
GDC 4	1.53	4.23	0.92	0.92	4.31	0.67
GDC 5	1.08	4.76	0.90	0.97	4.87	0.71
GDC 6	0.38	5.10	0.65	0.78	5.10	0.75
GDC 7	0.79	5.19	0.81	0.67	5.28	0.49

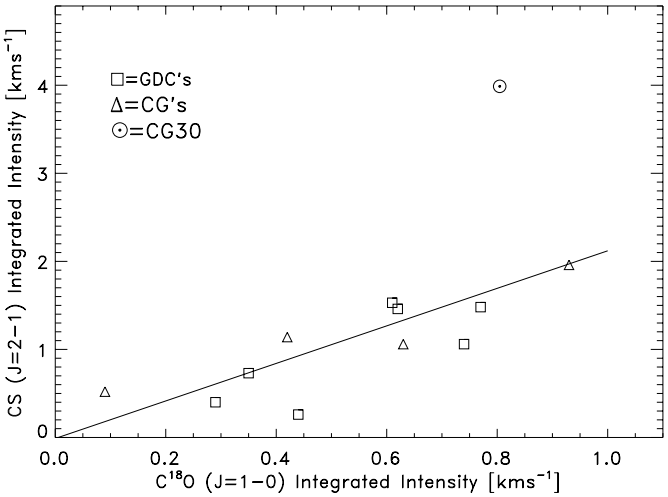

Fig. 6. The figure shows the integrated CS intensity plotted against $C^{18}O$ integrated intensity. The squares are the GDC's, triangles denotes the CG's, except for CG 30 which is indicated by a star. The straight line fits the CG's and GDC's very well, but CG 30 falls well above the line, indicating that the globule is centrally condensed.

4.3.3. Physical parameters of CG 30

Given the width of the head of the globule of 0.3 pc, we derive the values $N(H_2)$=3.30×10^{21} cm^{-2} and $n(H_2)$=3.6 ×10^3 cm^{-3} for the column density and number density, respectively. The value of the latter is probably about two to three orders of magnitude higher in the core where star formation is taking place. Therefore, the density must fall of rather quickly towards the edge of CG 30 in order to give a mean density of 10^3–10^4 cm^{-3}. A plot of integrated CS (J=2–1) intensities versus $C^{18}O$ (J=1–0) intensities supports the centrally condensed nature of the globule (Fig. 6). In this figure we have included observations made towards 7 GDC (Gum Dark Clouds, see Table 5), similar to the cometary globules, but lacking their prominent tails. CG 30 is the only globule to fall well above the straight line which otherwise fits the other globules reasonably well. This is consistent with a higher collisional excitation of the CS molecule because of a higher density.

We have used the following relation to convert the derived ^{13}CO integrated intensities into equivalent visual extinctions (Lada et al. (1994)):

$$N_{13} = 2.18 \pm 0.24 \times 10^{15} A_v \qquad A_v < 5 \tag{7}$$

The maximum value of the visual extinction towards the centre position of CG 30 is 4.2 mag and the minimum value is 3.4 mag. However, it is possible that the visual extinction is much higher towards the centre position if the telescope beam does not resolve all the structures present in the globule.

Fig. 7 is a contour plot of CG 30 showing the two different line components. The solid contour is the strong component (S.C) integrated in the velocity range from 2.2 to 7.1 km s^{-1}, and the dashed lines indicate the weak component (W.C) integrated from 7.1 to 12.6 km s^{-1}. The physical parameters derived for the two mass components are listed in Table. 4. From the presently available data it is not possible to decide if the small mass component is part of CG 30, or an independent globule, either in front or behind CG 30. The mass of the newly discovered globule, which we will call CG 30B, is close to 2 $M_\odot$. The linear, projected distance from IRS 4 to the centre of CG 30B, taken to be the position of maximum emission in ^{13}CO (-40,200), is 0.43 pc. A geometric mean diameter of CG 30B is 0.25 pc, which is even larger than CG 31B, and comparable to CG 30. The relative velocity between CG 30 and CG 30B is 4 km s^{-1}, almost an order of magnitude larger than the escape velocity for CG 30, indicating that CG 30B and CG 30 are not gravitationally bound.

The total mass of 10 $M_\odot$ is in agreement with the results obtained by Pettersson (1984) who found 16 $M_\odot$ based on a mean number density in the core of the globule of 10^5 cm^{-3}. From IR photometry Pettersson (1984) estimated a lower limit of the mass of CG 30 of 6.5 $M_\odot$, not far from our result.

4.3.4. The molecular outflow

In the ^{12}CO map, we have identified a molecular outflow originating from IRS 4 driving the HH 120 object. The area covered by the ^{12}CO observations is 3.7′×4.7′, but wing emission is not present everywhere. It is confined to the innermost 2′×2′ region, corresponding to 0.26×0.26 pc, at 450 pc. However, this region covers nearly the entire head of the globule (see Table 1). The maximum of redshifted wing emission is seen 20″ to the west of IRS 4. The same increase in wing emission towards the west is also supported by our observations of H_2CO (2_{12}–1_{11}), C_3H_2 (2_{12}–1_{01}) and CS in the two transitions J=2–1 and J=3–2 (Fig. 8, see Table 6 for line parameters), which all show broader widths than towards the central position, indicating that the outflow is stronger at (30,0). However, in agreement with the weak blueshifted emission seen in ^{12}CO, we have not been able to detect blue wing emission in any other molecule. The molecules mentioned above all have a dipole moment significantly larger than CO and demand a higher critical density. Therefore, we

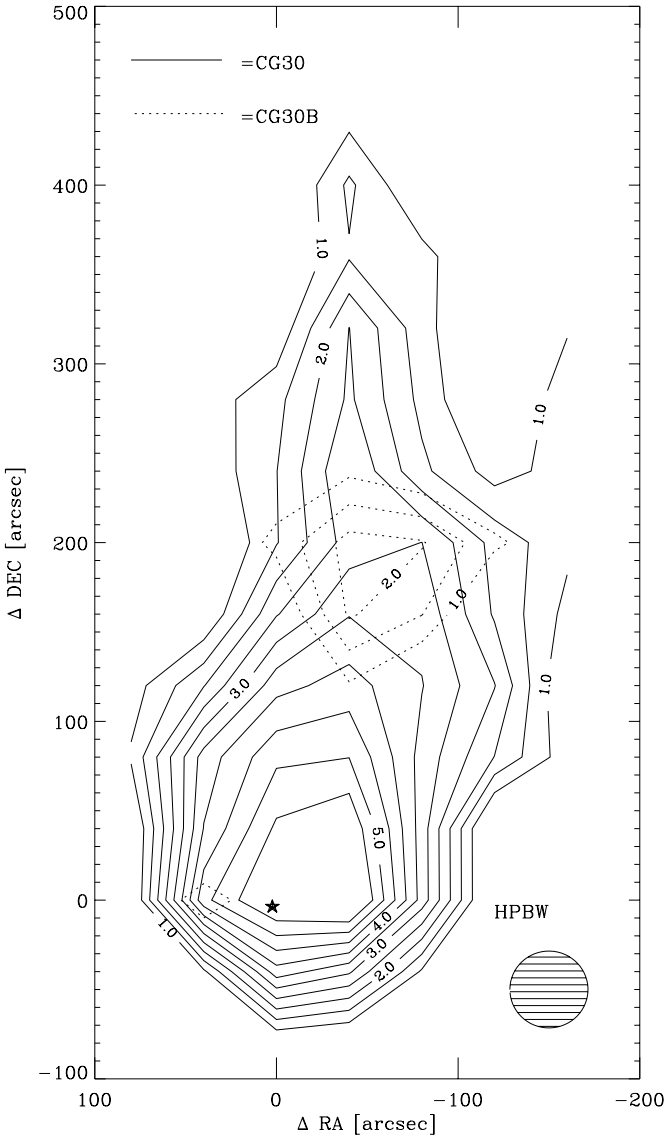

Fig. 7. A contour plot of the two distinct line components seen in the ^{13}CO spectra in CG 30. IRS 4 is located at (0,0). The solid contour is the main line integrated from 2.2 to 7.1 km s^{-1} (CG 30), and the dotted lines are integrated from 7.1 to 12.6 km s^{-1} (CG 30B). The lowest contour is 1 K km s^{-1} and the contour step size is 0.5 K km s^{-1}.

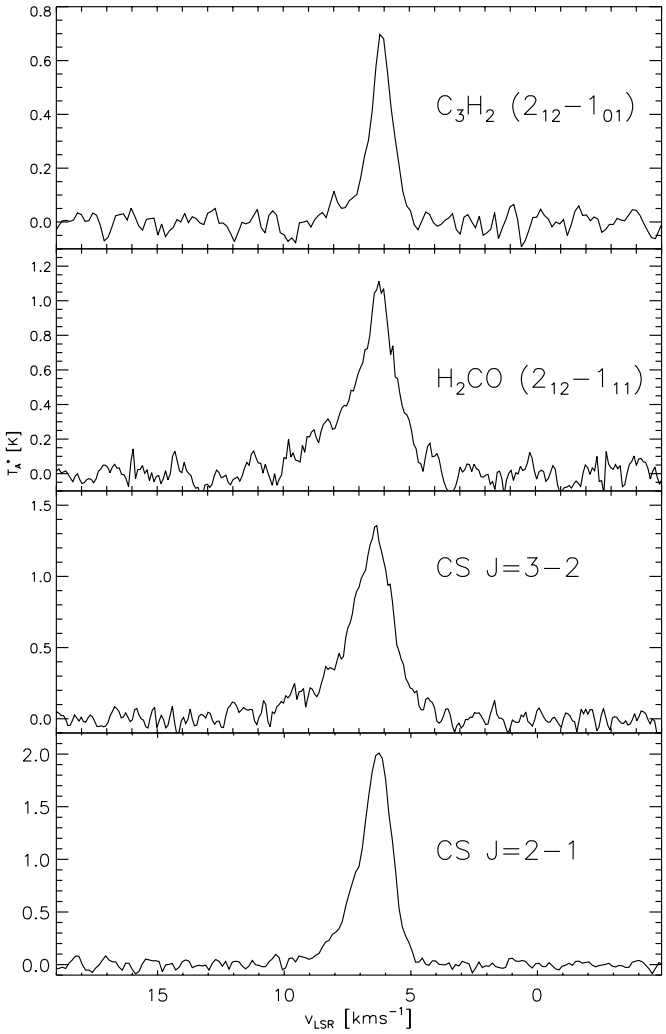

Fig. 8. Spectra of high dipole moment molecules observed towards maximum red wing emission (30,0). All profiles are characterised by red wing emission.

Table 6. Line parameters for observations towards CG 30 at the (0,0) and (30,0) positions.

Transition	Pos	$T_{\rm A}^*$	$\int T_{\rm A}^* dv$	Δv	$v_{\rm peak}$
CS (J=2–1)	(0,0)	2.41	3.89	1.61	6.32
CS (J=2–1)	(30,0)	2.01	3.32	1.67	6.47
CS (J=3–2)	(0,0)	1.90	3.27	1.70	6.13
CS (J=3–2)	(30,0)	1.37	2.97	2.17	6.79
H_2CO (2_{12}–1_{11})	(0,0)	1.90	3.27	1.70	6.13
H_2CO (2_{12}–1_{11})	(30,0)	1.37	2.98	2.17	6.79
C_3H_2 (2_{12}–1_{01})	(0,0)	0.94	1.09	1.08	6.03
C_3H_2 (2_{12}–1_{01})	(30,0)	0.79	0.75	1.15	6.08

conclude that HH 120 is in fact associated with a dense molecular outflow. The fact that we see wing emission in e.g. CS and not in the ^{13}CO spectra, is probably due to the poor signal to noise ratio in the ^{13}CO spectra.

In Fig. 9, a contour plot of the blue- and redshifted ^{12}CO emission is shown. We have integrated the blueshifted emission from -2 to 4.5 km s^{-1}, and the redshifted emission from 7 to 15 km s^{-1}. The blueshifted wing emission appears weak and smeared out. The redshifted emission, on the other hand, is characterised by a better defined lobe. We interpret this as a flow where the blueshifted material is breaking out of the cloud on its front side where there is little if any ambient material to keep it confined. In this picture the better collimated redshifted material bores its way into the cloud and therefore is confined and collimated by the gas and dust inside the globule. Despite the low degree of collimation seen in the blueshifted material, the highest contour in Fig. 9 outlines a lobe originating from the position of the infrared source (at (0,0)) and pointing in the opposite direction as the red lobe. A comparison of Fig. 4 and 9 indicates a flow perpendicular to the tail of CG 30.

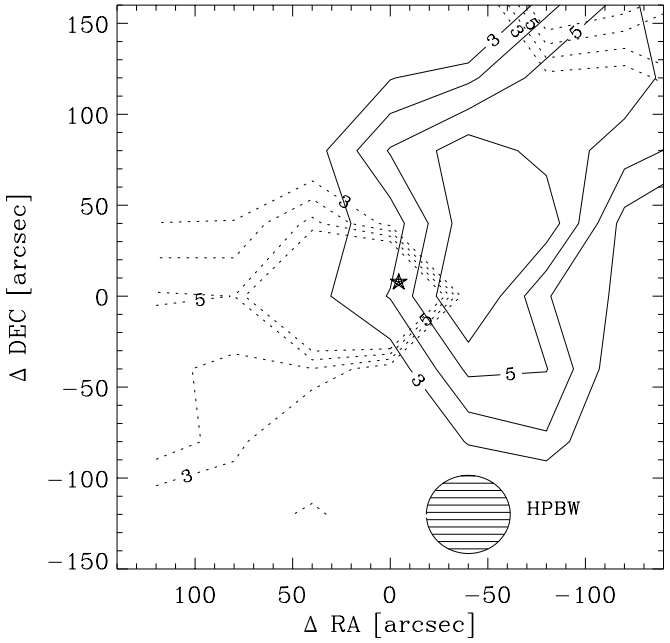

Fig. 9. A plot of the wing emission (^{12}CO (J=1–0)) for CG 30. IRS 4 is indicated by a star. The solid lines are the blueshifted wing emission (integrated from -2.0 to 4.5 km s^{-1}), and the dotted lines are the redshifted wing emission (integrated from 7.0 to 15.0 km s^{-1}), defined in Fig. 5. The redshifted wing emission is collimated, whereas the blueshifted emission is weak are smeared out. In the upper right corner some contours (dashed lines) of CG 30B are seen. The lowest contour is 1 K km s^{-1} and the step size is 1 K km s^{-1}.

Table 7. Outflow parameters

Gas	Vel. km/s	$\int T_A^* dv$ (K km/s)	N(^{12}CO) (cm^{-2})	N(H_2) (cm^{-2})	M ($M_\odot$)
Red	7 to 15	390	4.1×10^{17}	4.1×10^{21}	0.13
Blue	-2 to 4.5	394	4.2×10^{17}	4.2×10^{21}	0.14

Assuming that we are dealing with a molecular outflow, we can calculate some associated physical quantities which are presented in Table 8. We assume an excitation temperature of 12 K and optically thin emission in the line wings; we do not have any spectra in the higher transitions of ^{12}CO to check these assumptions. We have used Eq. 3 to calculate the ^{12}CO column density, with the constant replaced by 2.38×10^{14}. Using an abundance ratio of $[^{12}\mathrm{CO}]/[\mathrm{H_2}]=10^{-4}$ and integrating over all positions showing high velocity emission, we have calculated the masses of the blueshifted (-2 to 4.5 km s^{-1}) and redshifted (7 to 15 km s^{-1}) outflow, and corresponding dynamical parameters for a steady flow. Because the outflowing gas might be optically thick or at a higher excitation temperature than 15 K, our mass estimate will have to be considered as a lower limit (see e.g. Levreault 1988 for a discussion on the uncertainties in the mass determination of outflows). More seriously, we are unable to estimate the inclination angle of the flow. Without the inclination correction the calculated dynamical time scale is an upper limit, and the estimates of momentum and kinetic energy are likely to involve larger uncertainties than determination of flow mass. The maximum extent of the redshifted lobe measured from IRS 4 has been determined to be 0.15 pc, and the maximum velocity 9 km s^{-1}, taken to be the velocity of the flow. In Table 8, we list the derived dynamical flow parameters, where M is the total mass of the outflow, $P = MV_{\rm max}$ is the momentum, $t_{\rm dyn} = R/V_{\rm max}$ is the dynamical time scale, $E_{\rm kin} = \frac{1}{2}MV_{\rm max}^2$ is the kinetic energy, and $L_{\rm mech} = \frac{1}{2}MV_{\rm max}^2/t_{\rm dyn}$ is the mechanical luminosity (the energy supply rate) of the outflow. These numbers deviate (more than one order of magnitude) from what was calculated earlier by Olberg et al. (1989); they present a flow mass of 4.51 $M_\odot$, implying that the rest of the derived physical parameters will deviate as well. However, a rediscussion of the data seems to indicate that the derived values presented here are the correct ones. The flow mass and mechanical luminosity are at the lower end of the range known from compiled lists of molecular outflows (Lada 1985). We are aware that our numbers are uncertain, but if the dynamical time scale has the correct order of magnitude it seems reasonable to conclude that the IR source IRS 4 is a Class 0 object, as the infrared work by Persi et al. (1994) indicated. However, the interpretation of the dynamical time scale is rather controversial. According to Padman et al. (1997), t_{dyn} significantly underestimates the true age of the outflow and the embedded source. The mechanical luminosity is proportional to $V_{\rm max}^3$ and is therefore strongly dependent on the adopted value of the inclination angle. Assuming that the uncertainty in the velocity is a factor of 2, then, because of projection effects, the luminosity of the CG 30 flow could be greater by almost an order of magnitude and $t_{\rm dyn}$ even smaller than indicated in Table 8.

Table 8. Derived dynamical parameters of the outflow for $V_{\rm max}$ =9 km s^{-1}, and $R_{\rm max}$=0.15 pc.

M ($M_\odot$)	P ($M_\odot$ km s^{-1})	$t_{\rm dyn}$ (yr)	$E_{\rm kin}$ (erg)	$L_{\rm mech}$ ($L_\odot$)
0.27	2.43	1.7×10^4	2.2×10^{44}	0.11

In the case of CG 30 the mechanical energy of the flow ($L_{\rm mech}t_{\rm dyn}$=2.2×10^{44} erg) is larger than the gravitational energy of the globule (GM^2/R=6.7×10^{43} erg). It is therefore unlikely to be gravitationally bound or even close to virial equilibrium. We found the virial masses to be an order of magnitude larger than the computed ^{13}CO masses. It is therefore conceivable, that the flow could prevent further star formation in CG 30.

5. Conclusions

We have observed the cometary globules CG 30/31/38 in the Gum nebula in various isotopes of CO. In addition, the molecular outflow has been observed in higher dipole moment molecules like CS, H_2CO and C_3H_2. We obtained the following results:

1. The excitation temperature of the globules on the basis of CO observations is found to be between ∼5 and ∼14 K,

assuming LTE conditions for the transitions, in agreement with results typical for dense cores of gas and dust (Martin & Barrett 1978).

2. From ^{13}CO J=1–0 maps we have determined the total mass associated with the globules to be $\sim$43 $M_\odot$. This is considered as a lower limit because of uncertainties in the optical depth.
3. We see signs of possible fragmentation of CG 31A and CG 38, since their spectra show two distinct lines. According to earlier studies (Reipurth 1981) Rayleigh-Taylor and Kelvin-Helmholtz instabilities induced by strong stellar winds or UV radiation can disintegrate the larger globules and create small ones.
4. We have discovered that CG 30 seems to be associated with another globule having a mass close to 2 $M_\odot$ and moving with a velocity of 4 km s^{-1} relative to the rest of the globules in the complex. It is possible that this second globule, here named CG 30B, has been physically associated with CG 30 at earlier times, but is now totally released due to instabilities in the globule, in the same way as for CG 31A and CG 38. Unfortunately, due to scarcity of data, we are not capable of explaining a possible physical relation between CG 30B and CG 30. However, it offers a potential solution to the question of the evolution of angular momentum of a star forming globule.
5. From our ^{12}CO (J=1–0) observations we have detected a dense molecular outflow associated with CG 30. The masses of the red- and blueshifted emission are nearly equal to 0.14 $M_\odot$ each, resulting in a total mass of 0.28 $M_\odot$. This is under the assumption of optically thin emission, which is supported by the absence of wing emission in the ^{13}CO (J=1–0) lines. The redshifted emission seems to be collimated by the dense gas of its parental cloud, whereas the blueshifted emission is smeared out as the flow bursts out of the globule. Making no corrections for inclination effects and assuming a maximum observed velocity of 9 km s^{-1}, the molecular outflow has a dynamical age of 1.7×10^4 years and a mechanical luminosity of 0.11 $L_\odot$. Because the gravitational energy of the globule is less than the mechanical energy of the molecular outflow, the globule appears to be gravitationally unbound. The flow seems to be able to prevent further star formation.

Future investigations of ^{12}CO (J=2–1) spectra towards CG 30 are required in order to give a more precise estimate of the optical depth and the excitation conditions in the globule. This will allow a more precise mass estimate of the globule and the molecular outflow. Higher spatial resolution spectra of e.g. ^{12}CO (J=3–2), might reveal high velocity bullets associated with the outflow. Further line spectroscopic investigations are needed to address the issue of fragmentation and evolution of angular momentum of the double globule CG 30/30B.

Acknowledgements. The observations were made with the SEST at the European Southern Observatory and we would like to thank ESO for granting us time. The authors also wish to thank the SEST staff for valuable assistance during the observing runs. A. S. Nielsen wants to express his most sincere thank to Rammebevillingen 'Grundstofsyntese og dynamisk udvikling i vor galakse' for financial support. Special thanks to H. Jønch-Sørensen for helping producing Fig. 4.

References

Bertoldi F., 1989, ApJ 346, 735
Bertoldi F., McKee, C. F., 1990, ApJ 354, 529
Bhatt H. C., 1993, MNRAS 262, 812
Booth R. S., Delgado, G., Hagström, M. et al., 1989, A&A 216, 315
Brand P. W. J. L., Hawarden, T. G., Longmore, A. J., Williams, P. M., Caldwell, J. A. R., 1983, MNRAS 203, 215
Brandt J. C., Stecher, T. P., Crawford, D. L., Maran, S. P., 1971, ApJ 163, L99
Garden R. P., Hayashi, M., Gatley, I., Hasegawa, T., Kaifu, N., 1991, ApJ 374, 540
Graham J. A., 1986, ApJ 302, 352
Gum C. S., 1952, Observatory 72, 151
Hartley M., Manchester, R. N., Smith, R. M., Tritton, S. B., Goss, W. M., 1986, A&AS 63, 27
Hawarden T. G., Brand, P. W. J. L., 1976, MNRAS 426, 669
Kutner M. L., 1984, Fund. of. Cos. Phys. 9, 233
Kutner M. L., Ulich, B. L., 1981, ApJ 250, 341
Lada C. J., 1985, A&AR 23, 267
Lada C. J., Lada, E. A., Clemens, D. P., Bally, J., 1994, ApJ 429, 694
Lefloch B., Lazareff, B., 1994, A&A 289, 559
Lefloch B., Lazareff, B., 1995, A&A 301, 522
Leung C. M., Kutner, M. L., Mead, K.N., 1982, ApJ 262, 583
Levreault R. M., 1988, ApJ 329, 1041
Lynds B. T., 1962, ApJS 7, 1
Martin R. N., Barrett, A. H., 1978, ApJS 36, 1
Olberg M., Reipurth, B., Booth, R. S., 1989, Proceedings of the Symposium, Zermatt, Springer-Verlag, p. 120–124., 1989.
Oort J. H., Spitzer, L., 1955, ApJ 121, 6
Padman R., Bence, S., Richer, J., 1997, in *Herbig-Haro flows and the birth of low mass stars*, IAU symposium No. 182. ed. by B. Reipurth & Claude Bertout.
Persi P., Ferrari-Toniolo, M., Marenzi, A. R., et al., 1994, A&A 282, 233
Pettersson B., 1984, A&A 139, 135
Pottasch S. R., 1956, Bull. Astron. Inst. Netherlands 13, 77
Reipurth B., 1981, Cometary Globules in the Gum nebula, Master Thesis, University of Copenhagen
Reipurth B., 1983, A&A 117, 183
Reipurth B., Cernicharo, J, 1995, Rev. Mex. Astron. Astrofis. 1, 43
Sahu M. S., 1992, Ph.D. Thesis, University of Groningen
Sandquist Aa., 1976, MNRAS 177, 69p
Sridharan T. K., 1992, JA&A 13, 217
Zealey W. J., Ninkov, Z., Rice, E., Hartley, M., Tritton, S. B., 1983, Ap. lett. 23, 119